Comparative Medicine
Copyright 2021
by the American Association for Laboratory Animal Science

Vol 71, No 2
April 2021
Pages 116–122

Original Research

A 3D-printed Apparatus for Imaging Multiple Rats Simultaneously

Nicholas J Harrison,[1] Kate L Shumway,[2] Sarah A Hansen,[3] Charles A Maitz,[2] Lori A Thombs,[4] and Brian K Flesner[2,*]

CT (computerized tomography) is a necessary imaging modality for cancer staging and disease monitoring. Rodent models of cancer are commonly studied prior to human clinical trials, but CT in rodents can be difficult due to their small size and constant movement, which necessitates general anesthesia. Because microCT equipment is not always available, clinical CT may be a viable alternative. Limitations of microCT and clinical CT include biosecurity, anesthesia to limit image distortion due to motion, and cost. To address several of these constraints, we created a 3D-printed apparatus that accommodated simultaneous imaging of as many as 9 rats under gas anesthesia. Rats were anesthetized in series and placed in a 3 × 3 arrangement. To assess differences in attenuation between individual chambers and rows or columns in the device, we first imaged a standardized phantom plug as a control. We hypothesized that attenuation of specific rat organs would not be affected regardless of the location or position in the 3D-printed device. Four organs—liver, kidney, femur, and brain—were evaluated in 9 rats. For both the phantom and kidneys, statistically significant, but clinically negligible, effects on attenuation were noted between rows but not between columns. We attribute this finding to the absence of a top layer of the apparatus, which thus created asymmetric attenuation and beam hardening through the device. This apparatus allowed us to successfully image 9 rats simultaneously in a clinical CT machine, with negligible effects on attenuation. Planned improvements in this apparatus include completely enclosed versions for biosecure imaging.

Abbreviations: AAPM, American Association of Physicists in Medicine; CT, computerized tomography; HU, Hounsfield units; ROI, region of interest

DOI: 10.30802/AALAS-CM-20-000089

Preclinical studies routinely require the use of advanced diagnostic imaging techniques to evaluate animal models of human disease.[25] Longitudinal imaging studies with cohorts that are large enough to permit valid conclusions may be limited by cost and time factors. In addition, research institutions frequently use human equipment, necessitating strict pathogen exclusion measures.[16] Although microCT (computerized tomography) has been developed and used for high anatomic resolution of small animals, the equipment may be unavailable for use or difficult to access.[23] In addition, the high resolution (typically 50 to 100 um^3 voxel spacing) afforded by this equipment may not be necessary for a given experiment. A clinical CT machine (typical spatial resolution, 0.5 to 1.0 mm^3) may be an appropriate alternative in some situations. To overcome cost and time constraints, several multi-animal imaging devices have been created; however, they rely on injectable anesthesia.[10,33] This reliance can be challenging with regard to accurate monitoring of anesthesia in stacked or scaffold-style imaging devices, difficulty in redosing (if needed), and prolonged recovery times. Furthermore, the use of injectable anesthetics for CT has been associated with risk of corneal ulceration.[32] In contrast, inhalant anesthesia achieves rapid induction, is easy to adjust to maintain appropriate anesthetic depth, and allows a quick recovery.[6]

The majority of imaging devices described to date have been limited to use with mice.[10,33] Rats are the second most frequently used mammal in biomedical research and their popularity is growing due to advances in genome editing techniques, larger animal size, and physiologic parameters more similar to humans.[6] Improving the convenience and cost of imaging rats has the potential to advance preclinical study outcomes by facilitating longitudinal translational studies.

To address the challenges just described, we created a 3D-printed imaging device that would allow simultaneous imaging of multiple rats under inhalation anesthesia. After creating the device, we tested whether animals in that configuration could be scanned accurately without poor image quality or loss of detail. In any stacked or rotary device, the penetrating X-ray beam has to pass through multiple animals in various locations and scaffold materials. We tested whether our device would alter the attenuation of the X-ray beam and thus artifactually alter the image itself. A CT image is created by measuring the attenuation coefficient of various tissues; the attenuation is proportional to the tissue's electron density. Stated simply, attenuation of the X-ray beam is greater in tissues that have greater density. The densities are measured by using Hounsfield units (HU), where 0 HU equals water density. Tissues with a greater electron density than water have a positive HU value and appear brighter, and tissues with a lower electron density than water have a negative HU value and seem darker.[5] We hypothesized that the position

Received: 01 Oct 2020. Revision requested: 16 Dec 2020. Accepted: 19 Jan 2021.
Departments of [1]Veterinary Pathobiology and [2]Veterinary Medicine and Surgery, College of Veterinary Medicine, University of Missouri, Columbia, Missouri; [3]Office of Animal Resources, University of Missouri, Columbia, Missouri; and [4]Department of Statistics, College of Arts and Science, University of Missouri, Columbia, Missouri
[*]Corresponding author. Email: flesnerb@missouri.edu

of a rat in the apparatus would not affect the attenuation associated with specific organs (that is brain, liver, bone, and kidney). We also hypothesized that row and column would not affect the attenuation of a phantom control or organs.

Materials and Methods

Creating the apparatus. An 8-mo-old, intact male rat was measured for the development of the imaging bed. The tip of the nose to the tail base measured 21 cm, the tail itself was 16 cm long, and the height of the rat when prone was 3.75 cm. For repeat cylindrical printing, a commercially available water bottle (diameter, 6.5 cm; length, 24.5 cm) made of PVC plastic was determined to be the appropriate size and material. The label and adhesive material were removed with a commercially available product containing terpene hydrocarbons and C9–11 ethoxylated alcohols (Goo Gone, Weiman Products, Gurnee, IL). The base of the water bottle was sectioned and the edges sanded to prevent injury to animals, to a final length of 24 cm. A 20-mL syringe (Terumo, Tokyo, Japan) was transected at the 5-mL mark and inserted into the top of the bottle. To stabilize its attachment to the bottle, the syringe was secured in place by using a bead of glue (Gorilla Glue, Sharonville, OH) at the junction of the syringe and the lip of the bottle, thus completing the restraint device (Figure 1 A). We made 9 individual restraint devices.

To allow for flow-by anesthesia, a series of 24-in fluid extension sets (Baxter Healthcare, Deerfield, IL) were connected by using 4-way stopcocks and luer connections (Cole Parmer, Vernon Hills, IL), allowing simultaneous delivery of isoflurane to all 9 restraint devices. The nine 4-way stop-cocks were connected linearly, with a fluid extension set connected to each stopcock. This arrangement allowed attachment to each restraint device. An extension set was connected at each end of the line of stopcocks to allow connection to the anesthetic machine (Figure 1 B). A 5-mm uncuffed endotracheal tube was attached to a 4-way stopcock. The plastic connector of the endotracheal tube was removed, and approximately 1 cm of the tip of the tube was transected to make the end flat. The fluid extension set from each end of the line of stopcocks then was connected to the individual stopcock, completing the circuit and allowing for flow from both ends of the chain of stopcocks (Figure 1 C). The endotracheal tube was attached to the circuit of the anesthetic machine, allowing flow-by delivery of isoflurane to each rat during the imaging procedure.

A scaffold was created to hold modified water bottles in place during imaging. Modified water bottles were recreated by using an Autodesk Fusion 360 (San Rafael, CA). A 3D representation of the bottle was made, and 3 scaffolds were 3D-printed additively by using polylactic acid (0.3 mm layers, 10% infill, and 3 shells) on a Makerbot Z18 (MakerBot Industries, New York, NY). These devices were stacked, which allowed the anesthesia and scanning of as many as 9 animals simultaneously (Figure 1 D through F).

Measuring attenuation in each chamber: phantom plug. A phantom plug (0.99 HU; Gammex, Middleton, WI) was placed in the center of a cylindrical piece of Styrofoam (height, 2.54 cm; diameter, 6.5 cm; The Dow Chemical Company, MI). The plug within the Styrofoam was rotated through each of the 9 chambers. 1-mm collimated images of the scaffold were obtained at 100 kVp and 200 mAs on our Celesteion 16-slice PET–CT scanner (Canon, Ota, Tokyo, Japan). Three scans were performed for each location (27 scans total). Attenuation readings from regions of interest (ROI) were performed in triplicate by using MIM software (Cleveland, OH). A 1.2-cm ROI was used for each measurement and was verified by a senior radiology resident (KS).

Animals. This study was conducted in an AAALAC-accredited facility at the University of Missouri (Columbia, MO). All animals were maintained with practices consistent with the *Guide for the Care and Use of Laboratory Animals*.[13] All procedures were approved by the University of Missouri IACUC. Nine F344/DuCrl rats (age, 8 to 10 wk; Charles River Laboratory, Wilmington MA) were pair-housed with other rats from the colony in a conventional housing room, in ventilated caging (Ventilated Rat Rack, Thoren, Hazleton, PA). Aspen shavings (Northeastern Products Corp (Nepco), Warrensburg, NY) were used as bedding, and the water was acidified. They were fed a rodent diet (Labdiet 5008, Purina Mills International, St Louis, MO) ad libitum. The room and environmental parameters were monitored daily and maintained on a 12:12-h light:dark cycle. The rooms were maintained at temperatures between 68 and 79 °F (20.0 and 26.1 °C) and humidity between 30% and 70%. The rats were acclimated for 2 d prior to the CT procedure. The 9 rats and the colony were confirmed negative for fur mites and pinworms via PCR analysis and negative for Sendai virus, pneumonia virus of mice, sialodacryoadenitis virus, Kilham rat virus, H1 virus, rat parvovirus, rat minute virus, NS1 protein, rat theilovirus, *Mycoplasma pulmonis*, and *Pneumocystis carinii* via serology.

Measuring attenuation in each chamber: rats. Rats were anesthetized by using isoflurane anesthetic gas in an anesthetic induction chamber. Each animal was transferred from the induction chamber to an individual chamber in the apparatus. Three scans (100 kVp, 200 mAs) were performed; triplicate attenuation readings were performed for ROI of liver (5 mm parenchyma), bone (3 mm left head of femur), kidney (5 mm parenchyma), and brain (5 mm at left of temporomandibular joint). Kidney, liver, and brain were investigated to obtain the largest ROI for attenuation analysis; femur was chosen because of the very high density of mineralized bone. Total anesthetized time, from induction to recovery, was 15 to 20 min; the apparatus was mostly assembled prior to the rats' arrival in the CT imaging suite. Induction took 5 to 10 min. Rats spent 3 to 5 min being scanned and recovered from anesthesia within 5 min.

Statistics. For each of the 4 locations (liver, femur, kidney, brain,) a total of 9 measurements (3 replicates per 3 runs) were collected. To decrease variability, the response was computed as the average of the 3 replications, thus yielding 3 measurements per rat. Repeated-measures mixed-model ANOVA was used to determine whether statistically significant differences were present between the means of the 9 locations, which consisted of 3 rows and 3 columns, on the apparatus. After estimation of model parameters, residual diagnostic checks were performed to verify the normality assumption. When applicable, posthoc mean comparisons by using the Tukey method were conducted to determine which pairs of means differed.

Results

Feasibility of imaging rats. To determine the device's anesthetic feasibility, 9 rats were placed in the device and maintained throughout a CT imaging session (Figure 1 D and F). Rats were induced simultaneously in an induction chamber by using isoflurane inhalant anesthesia (1% to 5%) and an isoflurane vaporizer. Once the animals were deemed to be at an appropriate plane of anesthesia, they were moved to individual nosecones. All rats were maintained at an appropriate anesthetic plane with isoflurane anesthesia (1% to 5%) in the apparatus for the duration of the experiment. A second vaporizer was used for delivery into the apparatus in order to minimize time without anesthetic. The animals were maintained in the apparatus in a 3

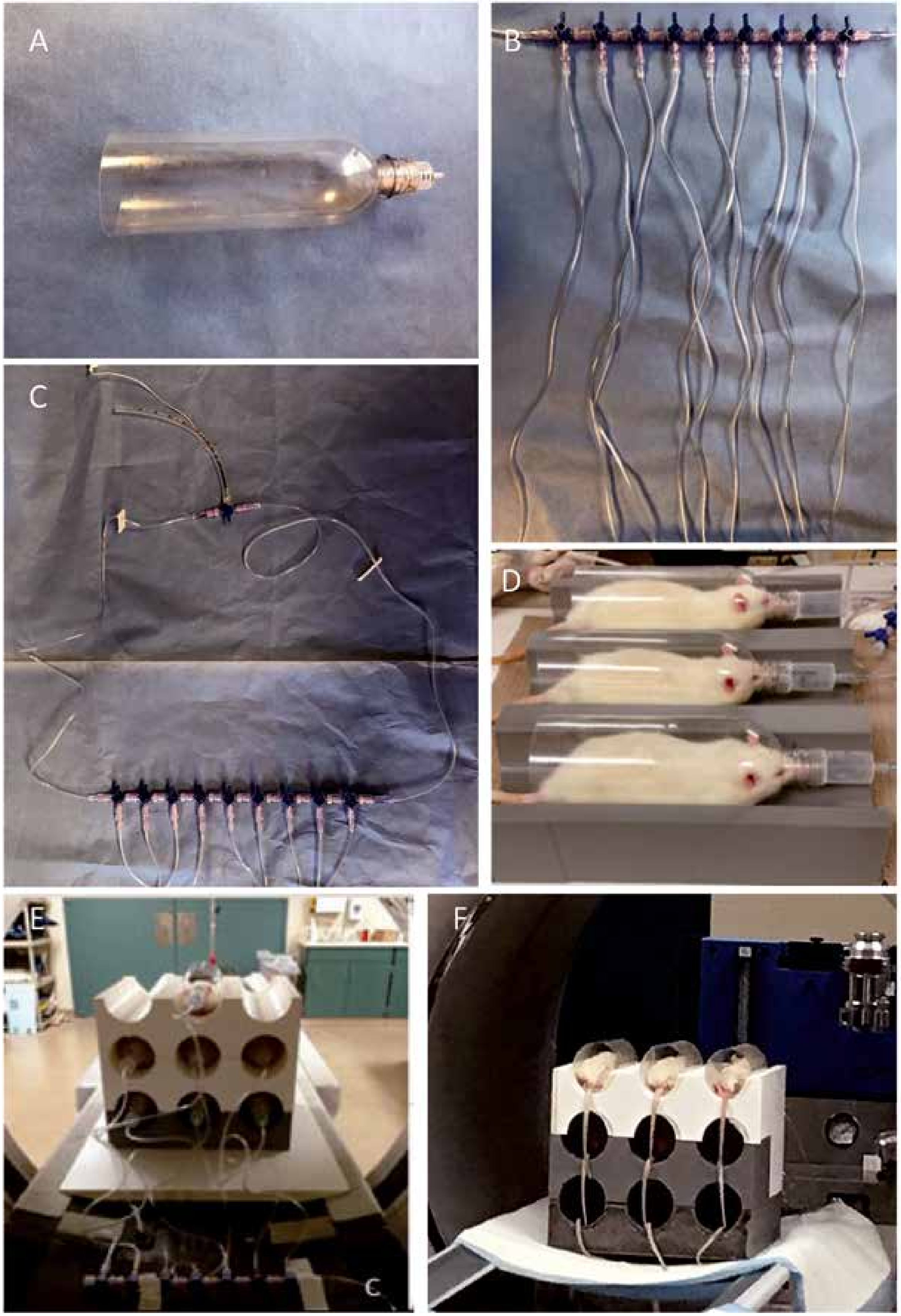

Figure 1. Components of the apparatus. (A) Plastic bottle restraint device. (B) Extension sets with 4-way stopcocks and extension sets in series. (C) Completion of anesthetic circuit. (D) Three rats anesthetized on the first row of the apparatus. (E) Completion of imaging of top row of anesthetized rats, with one rat anesthetized in the top middle position. (F) Nine rats under inhalant anesthesia and imaged on a clinical CT machine.

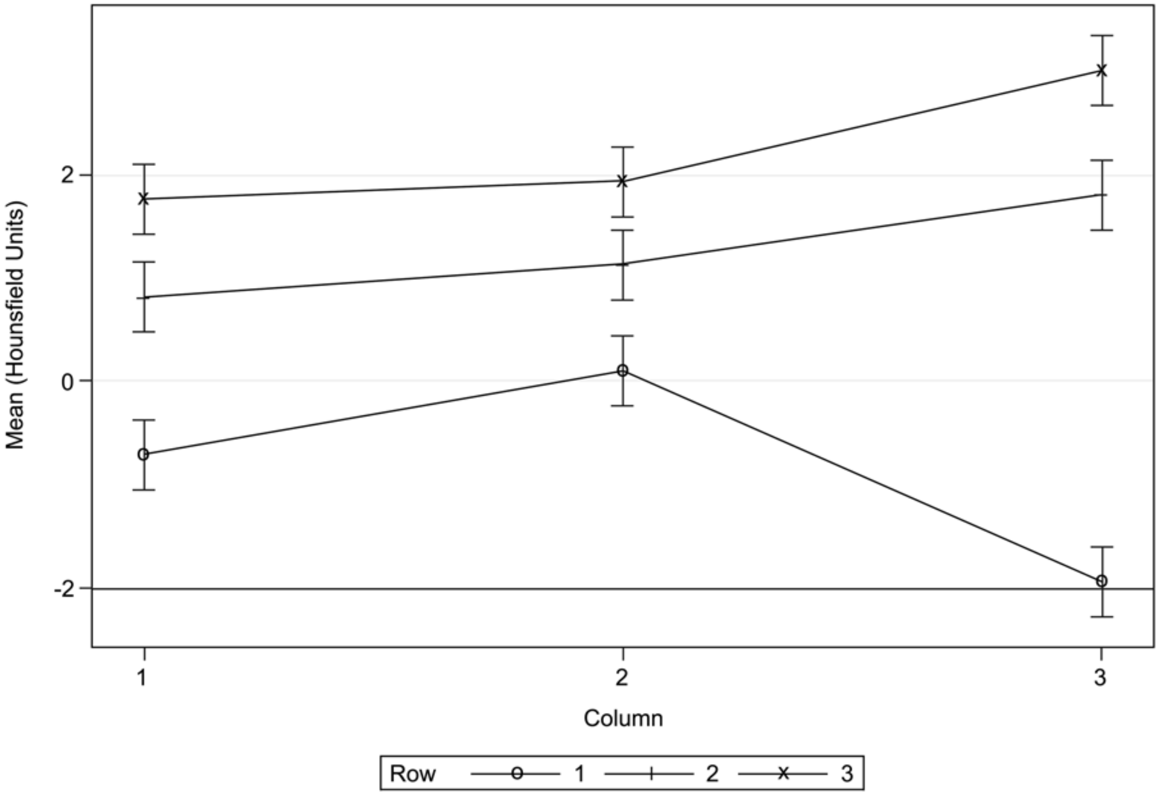

Figure 2. The phantom plug, with quality-assured attenuation of 1.0 HU, was placed in all 9 positions of the apparatus. This box and whisker plot shows the phantom in various positions in each row and subsequent column. Data points are the means of 3 separate runs for each position, with one confidence interval noted by the outer box; ranges are signified by whiskers. There was a significant ($P < 0.0001$) effect of row on attenuation (row averages, –0.84 to 2.2 HU), with row 1 significantly ($P < 0.0001$) different from each of the other 2 rows. There was no significant ($P = 0.23$) difference in attenuation between columns. Despite the statistically significant effect on attenuation between rows, these 1- to 2-HU changes are clinically insignificant.

× 3 configuration as described earlier; this configuration allowed for high throughput imaging (9 rats in one scan) with stable anesthesia and rapid recovery. Constant monitoring, which consisted of visual inspection and toe pinch, was possible due to the open nature of the apparatus. Titration of gas anesthetic could be performed between imaging sessions. All animals had a rapid recovery after discontinuation of isoflurane and recovered without incident. All images were obtained without movement artifact or interruption. All rats were deemed healthy via physical examination prior to and immediately after imaging. CT scans showed no evidence of pathology; however, rats were not euthanized nor was gross necropsy performed after conclusion of the imaging studies.

Effect of location on attenuation of the phantom plug. The phantom was placed in various positions (1 through 9) in the apparatus and imaged once per run. There was a statistically significant ($P < 0.0001$) effect of row (averages from –0.84 to 2.2 HU), with row 1 significantly ($P < 0.0001$) different from each of the other 2 rows. There was no statistically significant difference in attenuation between columns ($P = 0.23$). Attenuation of the phantom without the apparatus is 0.99 HU, as it is designed to represent integers relative to water (i.e., 0.0 HU). When we compared each mean with the average of the other 8 means, significant differences emerged for 2 means in row 1. Attenuation at several positions in row 1 and a single position in row 3 of the apparatus were significantly different from the average of the other means; however, these differences were within the HU tolerances prescribed by the American Association of Physicists in Medicine (AAPM63) and thus are not considered to be clinically significant (Figure 2).[21]

Changes in attenuation of various rat organs. Multiple soft tissue organs (liver, kidney, and brain) and one bone (femur) were evaluated (Figure 3). As in the phantom runs, a significant effect on attenuation (Figure 4) due to row position was noted for kidney ($P = 0.040$; row mean, 39.6 to 43.0 HU) but not for brain ($P = 0.38$; row mean, 33.0 to 34.9 HU), liver ($P = 0.097$; row mean, 67.3 to 70.9 HU), or femur ($P = 0.05$; row mean, 829.2 to 858.9 HU). No effect of column on attenuation was noted for any organ. Regardless of organ type, none of the 9 individual positions differed significantly from the average of all other positions.

Discussion

X-ray attenuation is quantified by measuring the fraction of radiation removed when passing through a given thickness of a specific material or tissue and depends on the electron density of the material. The signal is collected by a detector array, which generates light photons that are converted to an electric current. The electric current is calculated as the total linear attenuation coefficient of the tissues present within the X-ray path and is converted to HU.[31] When heterogeneous beams of photons are used, beams traveling through absorbing mediums become proportionately richer in high-energy photons, which is called beam hardening.[2] Photon beams traveling through the chamber at the center of the restraint device are likely to have more absorbing medium to pass through than at the sides, leading to beam hardening. When the object being imaged is noncircular

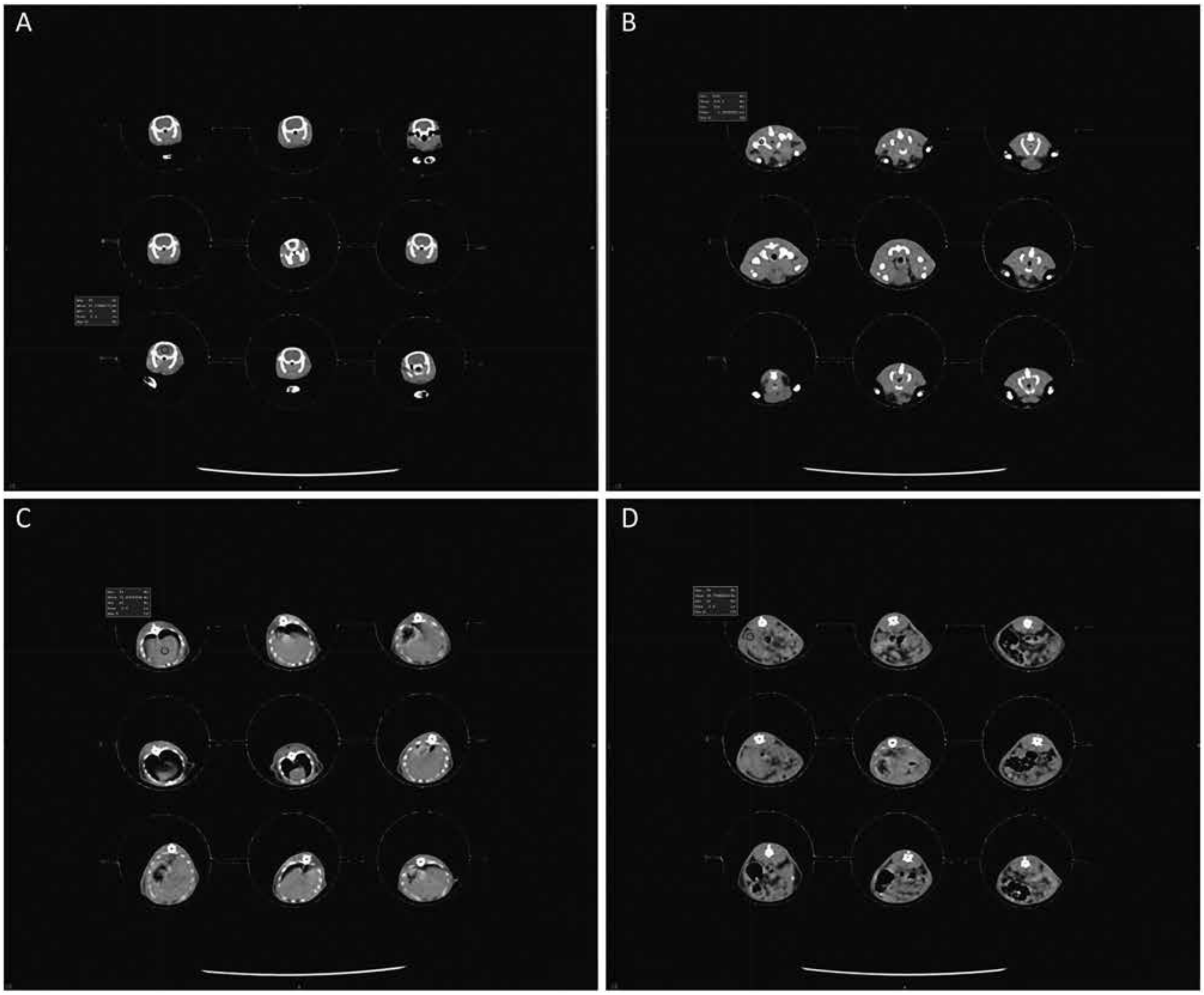

Figure 3. 2D images with various rat organs emphasized are (A) brain, (B) head of femur, (C) liver, and (D) kidney. Due to the small size of the rats and their related tissues, a small black circle can be seen in some slices; this is a region of interest (ROI) used to calculate attenuation (HU). Of note, all 9 rats are visualized in each slice; 9 black circles (ROI) are not noted in all rats, because care was taken to be precise in the calculation of HU from each tissue. Due to some positioning differences in rats, some organs may have been in a separate plane during image acquisition by using our 64-slice CT machine.

or asymmetric, the amount of material through which an X-ray beam passes may be inconsistent between projections, thus also affecting attenuation. The lack of a lid on our apparatus likely changed the X-ray path and contributed to beam hardening in other locations within the apparatus. This situation may have affected attenuation, but as previously mentioned, a range of 3 to 4 HU is within the 5-HU tolerance for CT scanners recommended by the AAPM Task Force 63 and therefore is unlikely to have clinical significance in the majority of animal tissues.[21] However, accounting for this effect is important when calibrating a CT machine if the apparatus was used during calibration.

A limitation of the current study is that the rats were not rotated among positions. Although they were an inbred strain and similar in age, some biologic and physiologic differences could nonetheless be present in individual rats. Liver, kidney, and brain were chosen as representative soft tissues and the head of the femur (increased attenuation due to lack of medullary cavity) was chosen for a bone comparator. Using the liver as a presumed homogeneous tissue has revealed attenuation differences between individual lobes.[22] These differences are likely due to disease processes like cancer or cirrhosis,[20,22,29] but nonpathologic states can also cause variation. For example, glycogen storage and compression of the organ by the ribs or diaphragm have been linked to transient differences in hepatic attenuation.[4,18,34] Specific to the kidneys, attenuation of human renal parenchyma can vary by 20 HU, with differences attributed to hydration status.[28] In the brain, changes in vascular perfusion are associated with changes in attenuation of the white matter,[26] and isoflurane has been shown to cause dose-dependent changes in cerebral blood flow.[19] We did not identify disease processes in any of the organs evaluated in the rats in the current study. However slight changes in positioning leading to organ compression and biologic differences due to glycogen storage, hydration status, or blood flow could affect attenuation and contribute to the differences observed.

Rats were well anesthetized within the apparatus, and no movement artifact was identified. As compared with injectable anesthesia, the use of inhaled isoflurane or sevoflurane limits motion artifact by delivering steady, continuous, stable anesthesia throughout the imaging time frame. However, the small diameter of the extension sets led to increased resistance in accordance with the Bernoulli principle. If this device is attached

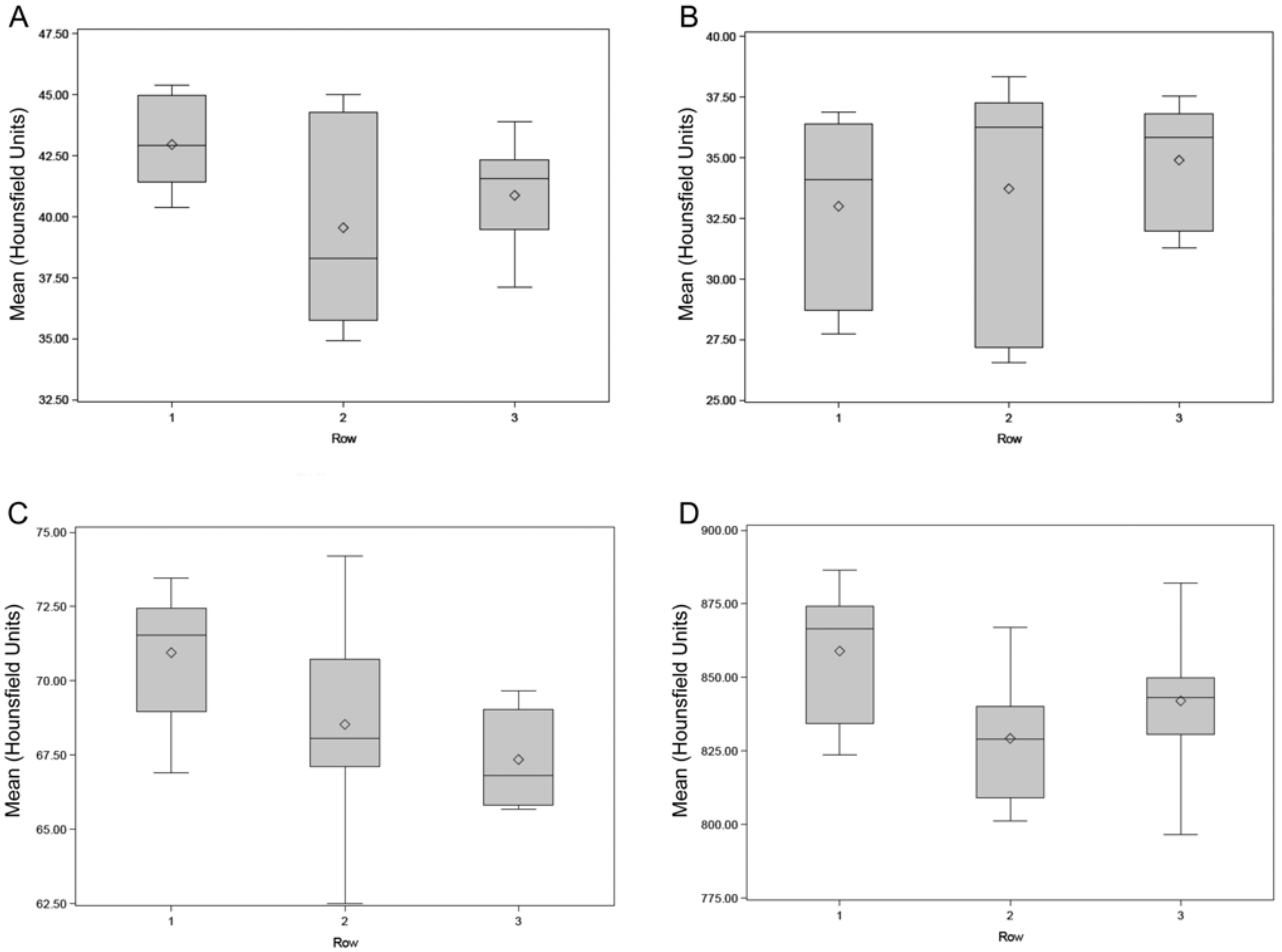

Figure 4. Box-and-whisker plots for (A) kidney, (B) brain, (C) liver, and (D) femur. Data points indicate the means of 3 separate runs for each position, with one confidence interval noted by the outer box; ranges are signified by whiskers. A statistically significant effect on attenuation due to row position was noted in kidney ($P = 0.040$; row means, 39.6 to 43.0 HU) but not in brain ($P = 0.38$; row means, 33.0 to 34.9 HU), liver ($P = 0.097$; row means, 67.3 to 70.9 HU), or femur ($P = 0.05$; row means, 829.2 to 858.9 HU). Despite the statistical significance between rows in attenuation in kidney, these small-magnitude HU changes are clinically insignificant.

directly to the breathing circuit on an anesthetic machine, the increased resistance in the small extension set lines will limit gas flow, and most of the anesthetic gas will escape through the extension valve. To overcome resistance, our anesthetic device must be attached directly to the oxygen inlet and gas outlet. This setup denies the gas an escape and overcomes the resistance in the smaller tubes, allowing for adequate gas flow. When the system is connected incorrectly, the rats will not be anesthetized appropriately, and motion artifact will occur.

The creation of a scavenging system is one of the next developmental steps for this device. Long-term occupational exposure to volatile anesthetic agents is thought to have adverse health effects on exposed personnel.[1,15,17] Although definitive evidence is available to support toxic effects due to isoflurane, potential teratogenic effects have had little investigation.[3] To limit exposure and meet OSHA guidelines (exposure limit of 2 ppm over 1 h of anesthetic administration), a scavenging system that collects halogenated anesthetic gases is needed.

Likewise, modifications to maintain strict biosecurity are essential. Barrier housing is often used to prevent unwanted infectious agents in research animals.[11] Barriers can be established at the cage, room, or facility level. For room or facility barriers, removing animals from the barrier and returning them from imaging suites that are located outside of the barrier increases the risk of barrier contamination.[11] Therefore, imaged animals are often euthanized; alternatively, they can be moved to a room outside the barrier to allow longitudinal studies. However, non-barrier areas may not use the same bedding, feed, PPE requirements, and water as are used in the barrier. Potential environmental changes and stress associated with relocation can alter the gut microbiome, thereby increasing variability and perhaps altering phenotype.[7,27,30] By creating a biosecure restraint device that can be sterilized chemically, animals could be moved to and from imaging suites or other areas outside the vivarium and yet still return to their original environment.

The creation of this device allowed us to anesthetize and image 9 rats quickly and efficiently with minimal effects on attenuation between animals. Therefore, we conclude that this device will contribute to longitudinal studies. Serial monitoring of animals is important for a variety of different experimental designs, including model phenotyping.[9,24] Compared with conventional CT, microCT designed for live animal imaging has a much higher spatial resolution (typically 50 to 100 µm^3 voxel spacing) that allows the evaluation of bone architecture and investigation of vasculature;[8,12,14] however, this level of detail may not be necessary for all studies. If the spatial resolution of a clinical CT device (0.5 to 1 mm^3 voxel) is sufficient, using our restraint apparatus will increase efficiency, reduce the time needed to perform imaging, and decrease overall study costs. In addition, with additional improvements to scavenge waste anesthetic gas and to enclose the device within a contained system, our apparatus has the potential to facilitate longitudinal studies that may not have been possible due to biosecurity issues.

References

1. **Basford AB, Fink BR.** 1968. The teratogenicity of halothane in the rat. Anesthesiology **29:**1167–1173. https://doi.org/10.1097/00000542-196811000-00014.
2. **Brooks RA, Di Chiro G.** 1976. Beam hardening in x-ray reconstructive tomography. Phys Med Biol **21:**390–398. https://doi.org/10.1088/0031-9155/21/3/004.
3. **Byhahn C, Wilke HJ, Westpphal K.** 2001. Occupational exposure to volatile anaesthetics: epidemiology and approaches to reducing the problem. CNS Drugs **15:**197–215. https://doi.org/10.2165/00023210-200115030-00004.
4. **Colagrande S, Centi N, La Villa G, Villari N.** 2004. Transient hepatic attenuation differences. AJR Am J Roentgenol **183:**459–464. https://doi.org/10.2214/ajr.183.2.1830459.
5. **DenOtter TD, Schubert J.** [Internet]. 2020. StatPearls [Internet]. Hounsfield unit. [Cited 3 September 2020]. Available at: https://www.ncbi.nlm.nih.gov/books/NBK547721/.
6. **Fox JG, Anderson LC, Otto G, Pritchett-Corning KR, Whary MT, editors.** 2015. Laboratory animal medicine. Amsterdam: Academic Press. https://doi.org/10.1016/B978-0-12-409527-4.00001-8
7. **Franklin CL, Ericsson AC.** 2017. Microbiota and reproducibility of rodent models. Lab Anim (NY) **46:**114–122. https://doi.org/10.1038/laban.1222.
8. **Garcia-Sanz A, Rodriguez-Barbero A, Bentley MD, Ritman EL, Romero JC.** 1998. Three-dimensional microcomputed tomography of renal vasculature in rats. Hypertension **31:**440–444. https://doi.org/10.1161/01.HYP.31.1.440.
9. **Guo Y, Zhang Y, Klein R, Nijm GM, Sahakian AV, Omary RA, Yang GY, Larson AC.** 2010. Irreversible electroporation therapy in the liver: longitudinal efficacy studies in a rat model of hepatocellular carcinoma. Cancer Res **70:**1555–1563. https://doi.org/10.1158/0008-5472.CAN-09-3067.
10. **Habte F, Ren G, Doyle TC, Liu H, Cheng Z, Paik DS.** 2013. Impact of a multiple mice holder on quantitation of high-throughput MicroPET imaging with and without Ct attenuation correction. Mol Imaging Biol **15:**569–575. https://doi.org/10.1007/s11307-012-0602-y.
11. **Hessler JR, Lehner NDM, editors.** 2009. Planning and designing research animal facilities. London: Academic Press.
12. **Holdsworth DW, Thornton MM.** 2002. Micro-CT in small animal and specimen imaging. Trends Biotechnol **20:**S34–S39. https://doi.org/10.1016/S0167-7799(02)02004-8.
13. **Institute for Laboratory Animal Research.** 2011. Guide for the care and use of laboratory animals, 8th ed. Washington (DC): National Academies Press.
14. **Kapadia RD, Stroup GB, Badger AM, Koller B, Levin JM, Coatney RW, Dodds RA, Liang X, Lark MW, Gowen M.** 1998. Applications of micro-CT and MR microscopy to study pre-clinical models of osteoporosis and osteoarthritis. Technol Health Care **6:**361–372. https://doi.org/10.3233/THC-1998-65-609.
15. **Klatskin G, Kimberg DV.** 1969. Recurrent hepatitis attributable to halothane sensitization in an anesthetist. N Engl J Med **280:**515–522. https://doi.org/10.1056/NEJM196903062801001.
16. **Klaunberg BA, Davis JA.** 2008. Considerations for laboratory animal imaging center design and setup. ILAR J **49:**4–16. https://doi.org/10.1093/ilar.49.1.4.
17. **Kramers PG, Burm AG.** 1979. Mutagenicity studies with halothane in Drosophila melanogaster. Anesthesiology **50:**510–513. https://doi.org/10.1097/00000542-197906000-00007.
18. **Leander P, Månsson S, Pettersson G.** 2000. Glycogen content in rat liver. Importance for CT and MR imaging. Acta Radiol **41:**92–96. https://doi.org/10.1258/rsmacta.41.1.92.
19. **Matta BF, Heath KJ, Tipping K, Summors AC.** 1999. Direct cerebral vasodilatory effects of sevoflurane and isoflurane. Anesthesiology **91:**677–680. https://doi.org/10.1097/00000542-199909000-00019.
20. **Mulhern CB Jr, Arger PH, Coleman BG, Stein GN.** 1979. Nonuniform attenuation in computed tomography study of the cirrhotic liver. Radiology **132:**399–402. https://doi.org/10.1148/132.2.399.
21. **Mutic S, Palta JR, Butker EK, Das IJ, Huq MS, Loo LN, Salter BJ, McCollough CH, Van Dyk J.** 2003. Quality assurance for computed-tomography simulators and the computed-tomography-simulation process: Report of the AAPM radiation therapy committee task group no. 66. Med Phys **30:**2762–2792. https://doi.org/10.1118/1.1609271.
22. **Nishikawa J, Itai Y, Tasaka A.** 1981. Lobar attenuation difference of the liver on computed tomography. Radiology **141:**725–728. https://doi.org/10.1148/radiology.141.3.6272353.
23. **Paulus MJ, Gleason SS, Kennel SJ, Hunsicker PR, Johnson DK.** 2000. High resolution X-ray computed tomography: an emerging tool for small animal cancer research. Neoplasia **2:**62–70. https://doi.org/10.1038/sj.neo.7900069.
24. **Peng S, Zhang G, Zhang BT, Guo B, He Y, Bakker AJ, Pan X, Zhen W, Hung L, Qin L, Leung WN.** 2013. The beneficial effect of icaritin on osteoporotic bone is dependent on the treatment initiation timing in adult ovariectomized rats. Bone **55:**230–240. https://doi.org/10.1016/j.bone.2013.02.012.
25. **Puaux AL, Ong LC, Jin Y, Teh I, Hong M, Chow PK, Golay X, Abastado JP.** 2011. A comparison of imaging techniques to monitor tumor growth and cancer progression in living animals. Int J Mol Imaging **2011:**1–12. https://doi.org/10.1155/2011/321538.
26. **Räihä UTS, Kurki T, Rajala T, Sourander L.** 1993. Relationship between vascular factors and white matter low attenuation of the brain. Acta Neurol Scand **87:**286–289. https://doi.org/10.1111/j.1600-0404.1993.tb05509.x.
27. **Ravussin Y, Koren O, Spor A, LeDuc C, Gutman R, Stombaugh J, Knight R, Ley RE, Leibel RL.** 2012. Responses of gut microbiota to diet composition and weight loss in lean and obese mice. Obesity (Silver Spring) **20:**738–747. https://doi.org/10.1038/oby.2011.111.
28. **Sagel SS, Stanley RJ, Levitt RG, Geisse G.** 1977. Computed tomography of the kidney. Radiology **124:**359–370. https://doi.org/10.1148/124.2.359.
29. **Scott WW Jr, Sanders RC, Siegelman SS.** 1980. Irregular fatty infiltration of the liver: diagnostic dilemmas. AJR Am J Roentgenol **135:**67–71. https://doi.org/10.2214/ajr.135.1.67.
30. **Tabata H, Kitamura T, Nagamatsu N.** 1998. Comparison of effects of restraint, cage transportation, anaesthesia and repeated bleeding on plasma glucose levels between mice and rats. Lab Anim **32:**143–148. https://doi.org/10.1258/002367798780599983.
31. **Thrall DE, editor.** 2013. Textbook of veterinary diagnostic radiology. St Louis (MO): Elsevier Saunders.
32. **Turner PV, Albassam MA.** 2005. Susceptibility of rats to corneal lesions after injectable anesthesia. Comp Med **55:**175–182.
33. **Yagi M, Arentsen L, Shanley RM, Hui SK.** 2014. High-throughput multiple-mouse imaging with micro-PET/CT for whole-skeleton assessment. Phys Med **30:**849–853. https://doi.org/10.1016/j.ejmp.2014.06.003.
34. **Yoshimitsu K, Honda H, Kuroiwa T, Irie H, Aibe H, Shinozaki K, Masuda K.** 2001. Unusual hemodynamics and pseudolesions of the noncirrhotic liver at CT. Radiographics **21 Suppl_1:**S81–S96. https://doi.org/10.1148/radiographics.21.suppl_1.g01oc06s81.